

Two-photon imaging of a magneto-fluorescent indicator for 3D optical magnetometry

Hohjai Lee,^{1,2,3} Daan Brinks,^{1,3} and Adam E. Cohen^{1,*}

¹*Department of Chemistry and Chemical Biology and Physics, Howard Hughes Medical Institute and Harvard University, Cambridge, MA 02138, USA*

²*Department of Chemistry, Gwangju Institute of Science and Technology, 123 Cheomdan-gwagiro, Bukgu, Gwangju 61005, South Korea*

³*These authors contributed equally to this work*

*cohen@chemistry.harvard.edu

Abstract: We developed an optical method to visualize the three-dimensional distribution of magnetic field strength around magnetic microstructures. We show that the two-photon-excited fluorescence of a chained donor-bridge-acceptor compound, phenanthrene-(CH₂)₁₂-O-(CH₂)₂-N,N-dimethylaniline, is sensitive to ambient magnetic field strength. A test structure is immersed in a solution of the magneto-fluorescent indicator and a custom two-photon microscope maps the fluorescence of this compound. The decay kinetics of the electronic excited state provide a measure of magnetic field that is insensitive to photobleaching, indicator concentration, or local variations in optical excitation or collection efficiency.

© 2015 Optical Society of America

OCIS codes: (160.3820) Magneto-optical materials; (180.2520) Fluorescence microscopy; (180.6900) Three-dimensional microscopy; (190.4180) Multiphoton processes; (350.5130) Photochemistry.

References and links

1. C. Chappert, A. Fert, and F. N. Van Dau, "The emergence of spin electronics in data storage," *Nat. Mater.* **6**(11), 813–823 (2007).
2. A. H. Lu, E. L. Salabas, and F. Schüth, "Magnetic nanoparticles: synthesis, protection, functionalization, and application," *Angew. Chem. Int. Ed. Engl.* **46**(8), 1222–1244 (2007).
3. B. B. Yellen, O. Hovorka, and G. Friedman, "Arranging matter by magnetic nanoparticle assemblers," *Proc. Natl. Acad. Sci. U.S.A.* **102**(25), 8860–8864 (2005).
4. A. Ito, M. Shinkai, H. Honda, and T. Kobayashi, "Medical application of functionalized magnetic nanoparticles," *J. Biosci. Bioeng.* **100**(1), 1–11 (2005).
5. V. V. Mody, A. Cox, S. Shah, A. Singh, W. Bevins, and H. Parihar, "Magnetic nanoparticle drug delivery systems for targeting tumor," *Appl. Nanosci.* **4**(4), 385–392 (2014).
6. R. Blakemore, "Magnetotactic bacteria," *Science* **190**(4212), 377–379 (1975).
7. J. L. Kirschvink and J. L. Gould, "Biogenic magnetite as a basis for magnetic field detection in animals," *Biosystems* **13**(3), 181–201 (1981).
8. J. L. Kirschvink, M. M. Walker, and C. E. Diebel, "Magnetite-based magnetoreception," *Curr. Opin. Neurobiol.* **11**(4), 462–467 (2001).
9. U. Hartmann, "A theoretical analysis of Bitter-pattern evolution," *J. Magn. Magn. Mater.* **68**(3), 298–304 (1987).
10. D. A. Allwood, G. Xiong, M. D. Cooke, and R. P. Cowburn, "Magneto-optical Kerr effect analysis of magnetic nanostructures," *J. Phys. D Appl. Phys.* **36**(18), 2175–2182 (2003).
11. M. Vengalattore, J. M. Higbie, S. R. Leslie, J. Guzman, L. E. Sadler, and D. M. Stamper-Kurn, "High-resolution magnetometry with a spinor Bose-Einstein condensate," *Phys. Rev. Lett.* **98**(20), 200801 (2007).
12. Y. Martin and H. K. Wickramasinghe, "Magnetic imaging by 'force microscopy' with 1000 Å Resolution," *Appl. Phys. Lett.* **50**(20), 1455 (1987).
13. J. R. Kirtley and J. P. Wikswo, Jr., "Scanning Squid Microscopy," *Annu. Rev. Mater. Sci.* **29**(1), 117–148 (1999).
14. A. M. Chang, H. D. Hallen, L. Harriott, H. F. Hess, H. L. Kao, J. Kwo, R. E. Miller, R. Wolfe, J. van der Ziel, and T. Y. Chang, "Scanning Hall probe microscopy," *Appl. Phys. Lett.* **61**(16), 1974 (1992).
15. L. M. Pham, D. Le Sage, P. L. Stanwix, T. K. Yeung, D. Glenn, A. Trifonov, P. Cappellaro, P. R. Hemmer, M. D. Lukin, H. Park, A. Yacoby, and R. L. Walsworth, "Magnetic field imaging with nitrogen-vacancy ensembles," *New J. Phys.* **13**(4), 045021 (2011).
16. H. Lee, N. Yang, and A. E. Cohen, "Mapping nanomagnetic fields using a radical pair reaction," *Nano Lett.*

- 11(12), 5367–5372 (2011).
17. C. A. Dodson, C. J. Wedge, M. Murakami, K. Maeda, M. I. Wallace, and P. J. Hore, “Fluorescence-detected magnetic field effects on radical pair reactions from femtolitre volumes,” *Chem. Commun. (Camb.)* **51**(38), 8023–8026 (2015).
 18. J. P. Beardmore, L. M. Antill, and J. R. Woodward, “Optical absorption and magnetic field effect based imaging of transient radicals,” *Angew. Chem.* **54**(29), 8494–8497 (2015).
 19. U. E. Steiner and T. Ulrich, “Magnetic field effects in chemical kinetics and related phenomena,” *Chem. Rev.* **89**(1), 51–147 (1989).
 20. K. Schulten, “Magnetic field effects in chemistry and biology,” *Adv. Solid State Phys.* **22**, 61–83 (1982).
 21. J. A. Jones and P. J. Hore, “Spin-selective reactions of radical pairs act as quantum measurements,” *Chem. Phys. Lett.* **488**(1–3), 90–93 (2010).
 22. K. Schulten, C. E. Swenberg, and A. Weller, “A biomagnetic sensory mechanism based on magnetic field modulated coherent electron spin motion,” *Z. Phys. Chem.* **111**(1), 1–5 (1978).
 23. K. Maeda, K. B. Henbest, F. Cintolesi, I. Kuprov, C. T. Rodgers, P. A. Liddell, D. Gust, C. R. Timmel, and P. J. Hore, “Chemical compass model of avian magnetoreception,” *Nature* **453**(7193), 387–390 (2008).
 24. H. Cao, Y. Fujiwara, T. Haino, Y. Fukazawa, C. H. Tung, and Y. Tanimoto, “Magnetic field effects on intramolecular exciplex fluorescence of chain-linked phenanthrene and *n*, *n*-dimethylaniline: influence of chain length, solvent, and temperature,” *Bull. Chem. Soc. Jpn.* **69**(10), 2801–2813 (1996).
 25. D. Brinks, A. J. Klein, and A. E. Cohen, “Two-Photon Lifetime Imaging of Voltage Indicating Proteins as a Probe of Absolute Membrane Voltage,” *Biophys. J.* **109**(5), 914–921 (2015).
 26. R. Ebrecht, C. Don Paul, and F. S. Wouters, “Fluorescence lifetime imaging microscopy in the medical sciences,” *Protoplasma* **251**(2), 293–305 (2014).
 27. M. Zhang, J. Chen, J. Gao, Z. Wang, H. Xu, M. Cai, J. Jiang, Z. Tian, and H. Wang, “Magnetic-field-enabled resolution enhancement in super-resolution imaging,” *Phys. Chem. Chem. Phys.* **17**(10), 6722–6727 (2015).
-

1. Introduction

Ever smaller and more complex magnetic components are an important part of data storage devices [1–3]. In medicine, magnetic nanoparticles are used as MRI contrast agents, in hyperthermic cancer treatments and for targeted drug delivery [4, 5]. Magnetotactic bacteria use magnetic nanoparticles to orient along Earth’s magnetic field lines [6], and magnetic sensing in fish and some birds has been hypothesized to depend on the presence of magnetite nanoparticles [7, 8].

The ability to visualize the magnetic field around micro- or nanostructures would aid in our understanding of and ability to control these structures. Techniques for 2D magnetic field imaging include Bitter pattern imaging [9], magneto-optical Kerr effect (MOKE) microscopy [10], and imaging with an atomic magnetometer [11]. Scanning techniques can, in principle, probe 3D field distributions. These include magnetic force microscopy (MFM) [12], scanning SQUID magnetometry [13], and scanning Hall effect microscopy [14]. However, the requirement for mechanical access limits the complexity of the topography that can be probed; and the requirement for mechanical scanning limits the time resolution. Recently, fluorescence-based techniques for optical magnetometry have been developed. Fluorescence from nitrogen vacancy centers in diamond has been used to map the magnetic field produced by magnetotactic bacteria [15], and fluorescence from a magnetic-sensitive dye has been used to map the magnetic field around ferromagnetic microstructures [16]. Recently, optical measurements of magnetic field effects in solution were performed using total internal reflection fluorescence (TIRF) [17]. However, these techniques mapped the magnetic field in a 2D plane strictly on one side of the sample. Optical measurements of magnetic fields in solution have also been performed using transient absorption on a solution of flavin adenine dinucleotide (FAD) [18]. Despite this progress, there remains a need for improved techniques to visualize microscopic 3D magnetic field distributions.

The magnetic field effect (MFE) in certain photochemical reactions provides an intriguing approach to monitoring nanoscale magnetic fields. The MFE arises from the action of the local magnetic field on the coherent precession of electron spins in a photogenerated spin-correlated radical pair [19]. In brief, a molecule with an electronic singlet ground state absorbs a photon. The photon drives electron transfer from a donor moiety to an acceptor moiety (either intra- or inter-molecular). The electrons become sufficiently separated that their spins do not interact, yet initially they preserve the spin coherence arising from their

starting singlet state. Each electron experiences a distinct set of hyperfine couplings to its surrounding protons, leading to gradual loss of coherence and intersystem crossing (ISC) into a triplet state. An external magnetic field can lock the precession of both electrons to the field axis, partially preserving the coherence and partially suppressing ISC [19–21]. In some chemical systems, the triplet state is non-fluorescent, while the singlet electron pair can recombine and emit light. Thus application of a magnetic field increases the fluorescence brightness. Magnetochemical effects are remarkable because they arise at magnetic field strengths comparable to the hyperfine energy (typically 1 – 10 mT), while the electron Zeeman splittings associated with these fields are $\sim 10^{-5} k_B T$ at room temperature. Magnetic field effects in photochemical reactions have been proposed as an alternative to nanoparticle-based physical compass mechanisms as a possible primary sensing mechanism for avian magnetoreception [22, 23].

Achieving sensitive magnetic field-dependent fluorescence requires achieving an optimal balance of the rates of intersystem crossing and radical pair recombination. Tethered donor-bridge-acceptor molecules in high dielectric constant solvents can show particularly large MFEs. The high dielectric constant solvent favors separation of the radical pair to enable independent and long-lived evolution of the spins; but the tether ensures that ultimately the radicals recombine rather than diffusing apart into the bulk. Cao and associates showed that the chained compound phenanthrene-(CH₂)₁₂-O-(CH₂)₂-*N,N*-dimethylaniline (Phen-12-O-2-DMA) underwent a > 2-fold increase in fluorescence between $B = 0$ and $B = 0.26$ T in rigorously degassed *N,N*-dimethyl formamide [24].

We previously applied Phen-12-O-2-DMA as a magnetic indicator and showed its use in quantitative mapping of magnetic fields around microfabricated metallic structures [16]. In the earlier work, we used a physical barrier to confine the magnetic indicator to a thin layer above the sample, to ensure that fluorescence was predominantly generated from within the nanoscale magnetic field above the sample. This confinement prevented 3D imaging of the magnetic field distribution.

Here, we show that two-photon-excited fluorescence of Phen-12-O-2-DMA also shows an MFE, and that this signal can be used for 3D optical mapping of magnetic field strength. We demonstrate this function by mapping the magnetic field around a fine iron wire. Measurements of the fluorescence lifetime via time-correlated single photon counting (TCSPC) provide an absolute measure of magnetic field strength that is insensitive to reporter concentration, photobleaching, illumination intensity, or fluorescence collection efficiency. We believe these measurements are the first two-photon measurements of a magnetic field effect in a radical pair system.

2. Methods

The magnetic indicator Phen-12-O-2-DMA (Fig. 1(a)) was synthesized following published procedures. The compound was characterized in earlier publications [16, 24]. The sample was dissolved in *N,N*-dimethyl formamide (DMF) at 1 mM concentration. To measure the two-photon-excited exciplex fluorescence as a function of magnetic field strength, we placed a home-built inverted epi-fluorescence microscope between the poles of a C-frame dipole electromagnet (GMW 5403) driven by a 400 W programmable bipolar power supply (KEPCO, BOP 20-20M). Femtosecond laser pulses (wavelength 710 nm, pulse width ~ 120 fs, repetition rate 80 MHz, and power 1 W) were focused on the sample in a #1-coverslip-bottomed sample cell through an air objective (Olympus, UplanSApo 40x, NA 0.95). Exciplex fluorescence was collected by the objective and separated from scattered excitation light by a 660 nm long pass dichroic mirror (Chroma, T660lpxrxt) and a bandpass filter centered at 500 nm with 140-nm bandwidth in front of a PMT (Hamamatsu, H10492). Magnetic field values were calibrated with a Hall effect sensor, with an estimated accuracy of 1% based on the measured magnetic field spatial profile and the precision with which the Hall

sensor was positioned and oriented. Signals were digitized and analyzed in Matlab. The apparatus was controlled via custom software written in LabView.

For 3D magnetic field imaging, the sample comprised a thin Fe wire (99.995%, Alfa Aesar), 2 mm long and 75 μm diameter. One end of the wire was affixed to a glass plate (1 cm diameter) by a drop of sodium silicate solution. The free end of the wire was bent upward at a $\sim 45^\circ$ angle. A sample chamber was formed by bonding a #1 coverslip to the bottom of a glass tube (2 cm diameter, 10 cm long) using sodium silicate (Fig. 1(b)). The plate with the wire was placed inverted in the sample chamber, so the free end of the wire rested on the coverslip. The sample was covered with solution of Phen-12-O-2-DMA in DMF, 1 mM. The sample chamber was capped with a rubber septum and the solution was bubbled continuously with N_2 gas. The bubbling created convection which carried heat and photochemical byproducts away from the high intensity laser focus, and protected the radical species from quenching by O_2 molecules.

A horizontal magnetic field was applied to the sample by a pair of permanent magnets (1 inch dia., 1 inch tall cylinder NdFeB) arranged on the sides of the sample chamber as in Fig. 1(b). The fringe fields magnetized the wire, leading to an inhomogeneous local field around the wire. The magnets were mounted on a motorized rotation stage (Thorlabs, PRM1-Z7) to change the orientation of the applied field and thereby to alter the local field distribution. The magnets were positioned such that the field strength at the wire was ~ 10 mT, corresponding to the field strength at which the magnetic indicator shows maximum sensitivity.

The two-photon (2P) imaging apparatus is shown in Fig. 1(c). A home-built beam-scanning two-photon microscope was used for the 3D magnetic field imaging. Excitation light was provided by a Spectra Physics Insight DeepSee laser, with pulses of ~ 120 fs at 80 MHz repetition rate. The maximum one-photon MFE occurred at $\lambda_{\text{exc}} = 308$ nm, and there was a sharp cutoff in the MFE at $\lambda_{\text{exc}} > 360$ nm [16], corresponding to a 2P excitation wavelength of 720 nm. To achieve a balance between maximizing the output power of the laser and maximizing the magnitude of the MFE, we operated the system with 710 nm excitation. The pulse dispersion was adjusted via an internal, motorized prism pair compressor controlled by Spectra Physics software.

The excitation light was steered by a pair of galvo mirrors (Cambridge Technology, 6215HM40B) onto the back aperture of an Olympus water immersion objective (UPLANSAPO 60x W, NA 1.2). The focal plane was selected by moving the objective axially with a linear stage (Thorlabs, MTS25-Z8). The exciplex emission at wavelengths shorter than 660 nm was separated from back-scattered excitation by reflection off a Semrock 660-nm long-pass dichroic (FF660-Di02-25x36). Residual laser light was rejected using a 500-nm bandpass filter with 140-nm bandwidth. The back aperture of the objective was reimaged onto a Hamamatsu R943-02 PMT operated in photon counting mode. To minimize dark-counts, the PMT was cooled to -20°C (PC104CE cooler, Pfr Technologies). Single-photon pulses were digitized using a Hamamatsu C9477 photon counting unit and counted with a National Instruments PCIe 6259 board.

Dispersion in the high NA objective can undesirably broaden the excitation pulse, leading to a loss of peak intensity. We minimized the pulse length in the focal plane by maximizing the two-photon fluorescence of a test sample (Constellation Microspheres, Life Technologies) as a function of the position of the dispersion-compensating prisms.

The secondary output beam of the Insight DeepSee laser ($\lambda = 1040$ nm) provided reference pulses for lifetime measurements. Pulses were detected using an ultrafast photodiode (Thorlabs, Det10A). Single-photon pulses from the PMT were digitized (Hamamatsu, C9477 photon counting unit), and then inverted using a Picoquant inverter. Reference and signal pulses were fed into a time correlated single photon counter (TCSPC, PicoHarp 300H, Picoquant). Reference and signal pulses were synchronized by changing the length of coaxial cable between photodiode and TCSPC unit. Fluorescence lifetime and

imaging data were synchronized by inserting into the photon record electronic markers at the start of each frame.

In a typical experiment, the sample was imaged in raster scan mode at a sampling rate of 10^5 pixels/s, in an area of $200 \times 200 \mu\text{m}$, at 512×512 pixel resolution, corresponding to a frame rate of 0.4 Hz. Average laser power was 40 mW, as measured after the objective. For a diffraction-limited focal area (500 nm diameter) the time-average intensity at the laser focus was 20 MW/cm^2 . Images of 2P-excited fluorescence and fluorescence lifetime were recorded as a function of orientation of the permanent magnet pair. 50 to 100 frames were averaged for each orientation of the magnet.

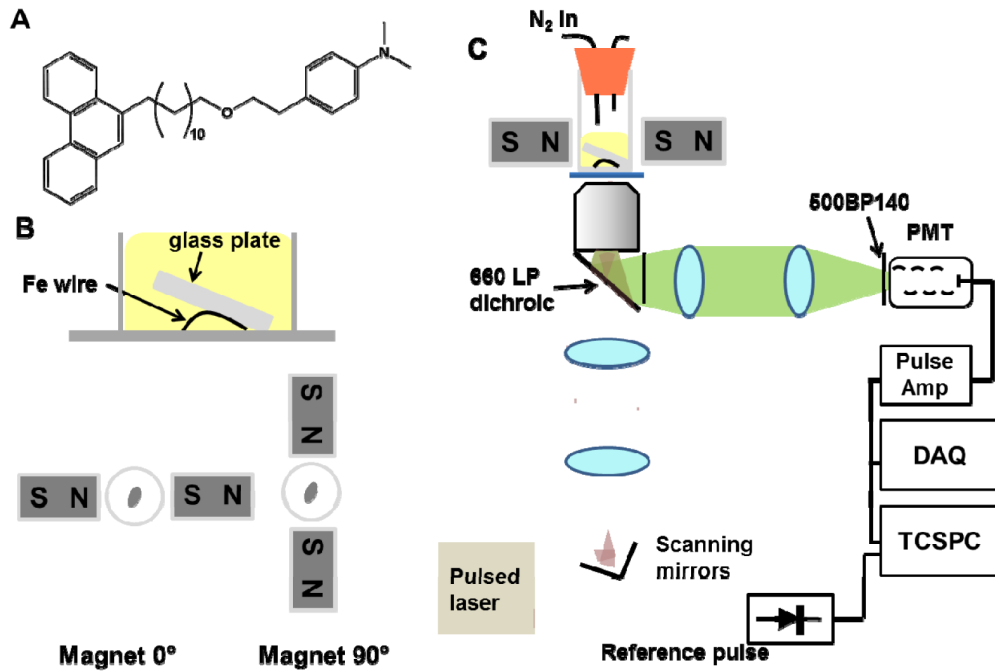


Fig. 1. Apparatus for 2-photon magnetic field imaging. A) Magneto-fluorescent indicator, Phen-12-O-2-DMA. B) Sample geometry. Top: side view of the sample chamber. The glass plate ensured that the Fe wire did not move in the applied magnetic field. Bottom: top view of the sample chamber showing the arrangement of the permanent magnets and the elliptical cross-section of the Fe wire in the center of the chamber. C) Two-photon imaging apparatus. Abbreviations explained in the main text.

3. Results

Figure 2 shows steady-state one- and two-photon fluorescence of Phen-12-O-2-DMA as a function of magnetic field. We define the MFE as the fractional change in fluorescence induced by the magnetic field,

$$MFE = \frac{F_B - F_0}{F_0}, \quad (1)$$

where F_B is the fluorescence with the magnetic field and F_0 is the fluorescence with no magnetic field. The one-photon- (adapted from Ref. 15) and two-photon-excited exciplex fluorescence showed similar magnetic field dependencies. The slightly smaller maximum MFE of two-photon excitation was likely due to two-photon excitation of magnetic field-insensitive background fluorescence. In both cases the MFE had greatest sensitivity between 8 and 15 mT. The emission spectrum of Phen-12-O-2-DMA, recorded with 355 nm excitation,

showed a broad emission band, peaked at 500 nm, which was sensitive to the applied magnetic field [16]. This band arose from exciplex emission from a loosely bound electron donor (DMA⁺) – electron acceptor (Phen⁻) complex. A sharp emission feature at 425 nm arose from prompt fluorescence and was not sensitive to magnetic field [16].

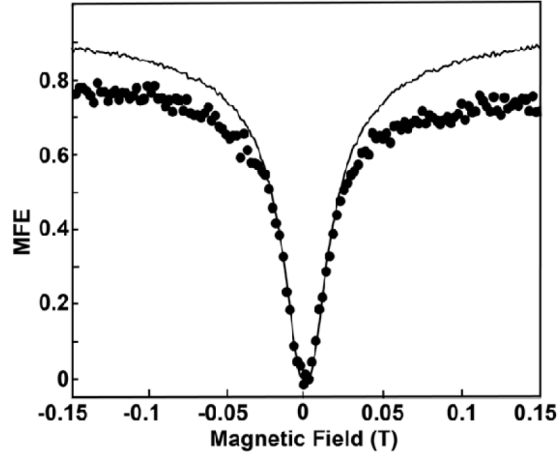


Fig. 2. Magnetic Field Effect of Phen-12-O-2-DMA. Steady-state fluorescence change, normalized to fluorescence at $B = 0$, as a function of magnetic field ($\lambda_{em} = 430 - 570$ nm). Line is for one-photon excitation ($\lambda_{exc} = 355$ nm) and dots are for two-photon excitation ($\lambda_{exc} = 710$ nm).

Degassed solution of Phen-12-O-2-DMA in DMF showed strong 2P fluorescence when excited at $\lambda_{exc} = 710$ nm. We imaged the fluorescence around a $75 \mu\text{m}$ Fe wire with 500 nm spatial resolution in the x - y plane and $10 \mu\text{m}$ step sizes in the z -direction. We observed a spatially dependent fluorescence amplitude. To determine whether these spatial variations arose from local variations in the magnetic field or from local variations in fluorescence excitation or collection efficiency, we acquired sets of images with the external magnets in different orientations. Rotation of the external magnets did not affect the mechanical or optical configuration of the sample, so changes in 2P fluorescence were necessarily from local changes in magnetic field. We define the fluorescence as a function of 3D coordinate \mathbf{r} and magnet rotation θ as $I(\mathbf{r}, \theta)$.

To quantify these fluorescence maps, we compared $I(\mathbf{r}, \theta)$ to $\langle I(\mathbf{r}, \theta) \rangle_{\theta}$, where $\langle \rangle_{\theta}$ indicates an average over the four orientations of the external magnets (0° , 90° , 180° , and 270°). We defined the relative MFE as:

$$MFE(\mathbf{r}, \theta) = \frac{I(\mathbf{r}, \theta) - \langle I(\mathbf{r}, \theta) \rangle_{\theta}}{\langle I(\mathbf{r}, \theta) \rangle_{\theta}}. \quad (2)$$

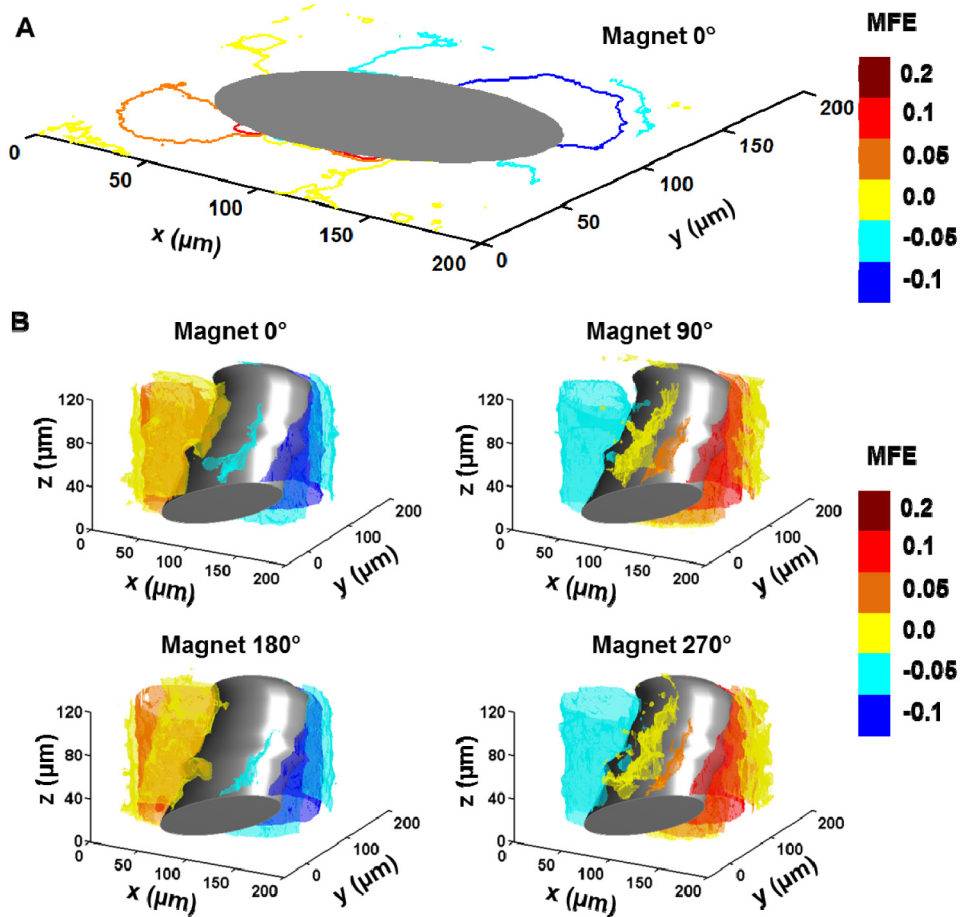


Fig. 3. 3D mapping of MFE around an iron wire. A) Contours of MFE strength in a slice imaged around the Fe wire at $z = 50 \mu\text{m}$. B) 3-dimensional mapping of the MFE around a section of Fe wire. Contours represent surfaces of constant MFE strength. Images were acquired with $\delta z = 10 \mu\text{m}$ between sections, and 500 nm in-plane spatial resolution.

The subtraction and division were performed pixel by pixel. Figure 3 shows 3D fluorescence maps of $MFE(\mathbf{r}, \theta)$ in the magnetic indicator solution around the Fe wire. By normalizing the fluorescence changes to the mean fluorescence, these maps are insensitive to position- or depth-dependent variations in optical excitation efficiency or fluorescence collection efficiency. This normalization is important because partial shadowing by the Fe wire could lead to spatially dependent fluorescence signals. Optical aberrations can also distort the excitation focal spot, leading to decreases in fluorescence signal at the periphery of the field of view and deep in the solution. The price for the normalization in Eq. (2) is that the signal no longer reflects the absolute strength of the magnetic field; rather it reflects the change in field strength due to rotation of the magnets. For structures with a permanent remnant magnetization, the MFE due to this static field will not be detected by this analysis protocol.

The precision with which the magnetic field could be measured was limited by the noise in the 2P fluorescence measurements. Typical fluorescence count rates at the detector were 4×10^5 counts/s, with approximately $N = 200$ counts contributing to the signal at each pixel. The Poissonian shot noise at each pixel was thus $N^{1/2} = 14$ counts. In an analysis of an image region where there was no magnetic field variation, we observed a pixel-to-pixel standard

deviation in intensity of 14.3 counts, indicating that the measurement precision was shot noise limited.

With static fluorescence, it is not possible to distinguish between signal variations from static magnetic fields and signal variations from optical artifacts. Encoding of magnetic field information into a time-domain signal provides a means to address this challenge, because time can be measured far more accurately than fluorescence intensity. We reasoned that the magnetic field would likely affect the fluorescence decay kinetics of the electronically excited molecule. Measurements of these kinetics would probe absolute magnetic field, without contamination from sources of variation in fluorescence magnitude. Similar strategies have been used in fluorescence lifetime imaging microscopy (FLIM) for many types of absolute measurements [25, 26].

We used a time correlated single photon counting (TCSPC) system to map the distribution of delays between 2P excitation and fluorescence emission. Figure 4(a) shows that Phen-12-O-2-DMA displays complex decay kinetics with a fast emission decay corresponding to a lifetime of ~ 4 ns, and a slow emission decay providing a plateau after 6 ns. A two-component fluorescence decay of Phen-12-O-2-DMA was previously reported with one-photon excitation [24]. The 80 MHz repetition rate of the laser prevented lifetime measurements at delays greater than 12.5 ns. The ratio of slow to fast emission components changed as a function of magnetic field, confirming that this quantity could serve as an absolute magnetic field reporter.

Figure 4 shows maps of the ratio of slow to fast fluorescence decay in a single plane around the Fe wire. A change in the characteristic pattern around the wire was observed when the magnets were put in place and rotated (Figs. 4(b)-4(d)). These results confirm that fast time correlated single photon counting, combined with two-photon excitation, can be used to record MFE images without the need for a reference.

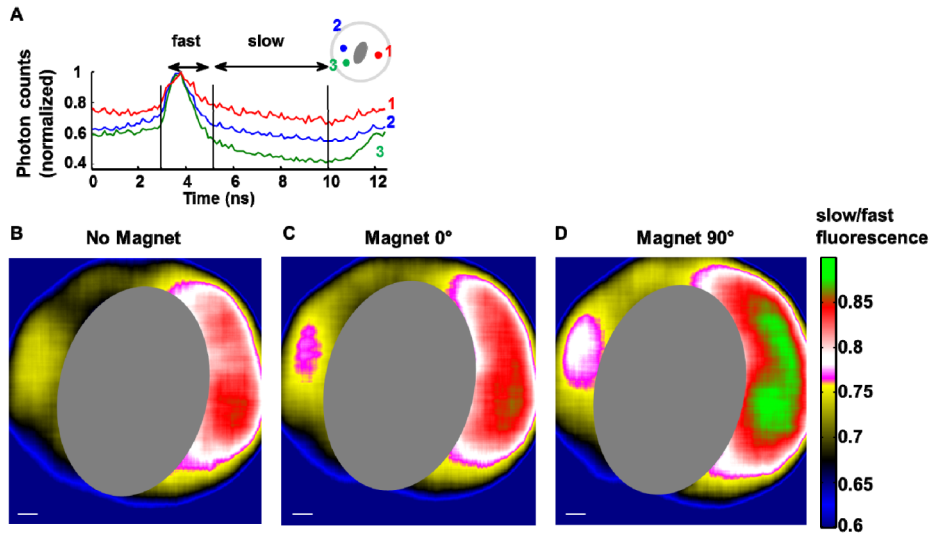


Fig. 4. MFE mapped with 2-photon-excited time correlated single photon counting. A) Histogram of arrival times relative to the excitation pulse at $t = 4$ ns for three locations around the wire with different magnetic field strengths. B-D) Images of the ratio of slow to fast fluorescence counts. This ratio reports local magnetic field without need for a reference image. Scale bars 10 μm .

4. Conclusion

We have shown that the magnetic field indicator Phen-12-O-2-DMA retains the magnetic field effect under two-photon excitation. We used this property to map the magnetic field

around an iron wire in three dimensions. Lifetime imaging provides a means to map the MFE without the need for reference images. The combination of two-photon excitation and fast time-correlated single photon counting provides a promising route towards 3D mapping of magnetic fields.

The key technical limitations to widespread use of fluorescent indicators for magnetic field mapping are their poor physico-chemical properties. The DMF solvent for Phen-12-O-2-DMA is not compatible with many organic polymers, necessitating the use of great care in preparing solutions and selecting a sample and imaging chamber. Additionally, the fluorescence of this compound is quite dim on a per-molecule basis, requiring a 1 mM solution to achieve adequate signal. A recent report of an MFE in the fluorescence of an excellent water-soluble dye, Cy5, is thus very encouraging [27]. The MFE of flavin adenine dinucleotide (FAD), a key component in a possible bio-magnetic sensor, was recently measured by total internal reflection fluorescence (TIRF) microscopy [17] and also imaged by transient optical absorption detection (TOAD) imaging technique [18]. Development of water-soluble compounds that show bright fluorescence and a large MFE is the paramount challenge for further development of the technology.

Liquid solutions are isotropic, so they only probe magnetic field magnitude, not direction. In some circumstances one might like to map the vector magnetic field. For samples with high magnetic coercivity, one could map the field direction by sequentially applying small external fields along each of the Cartesian axes. The extent to which the external field along each axis adds or subtracts from the field magnitude provides a measure of the projection of the sample's magnetic field along that axis.

Acknowledgments

We thank Rohini Shivamoggi, Vijay Jain, Ryan Spoering, Michael Campbell, and Tobias Ritter for help with chemical synthesis. This work was supported by an Office of Naval Research PECASE Award N00014-11-1-0549. HL acknowledges the support by the GIST Specialized Research Project (K05040), the Integrative Aging Research Center of GIST, and the Basic Science Research Program (NRF-2014R1A1A2056255). DB acknowledges support by a Rubicon Grant of the Netherlands Organization for Scientific Research (NWO).